Materials Advances

ROYAL SOCIETY OF CHEMISTRY

PAPER

View Article Online
View Journal | View Issue



Cite this: *Mater. Adv.*, 2025, 6, 3264

# Environmental materials: $CO_2$-adsorbing clays for enhancing soil fertility and agricultural sustainability†

Faizah Altaf,[a] Shakeel Ahmed,[b] Shahid Ali,[a] Muhammad Mansha[a] and Safyan Akram Khan*[a]

To combat desertification and climate change, innovative solutions are crucial for restoring the fertility of desert lands and mitigating the adverse effects of global warming. One promising approach involves utilizing carbon dioxide ($CO_2$), a major greenhouse gas, as a resource to enhance soil fertility. This study explores the transformation of desert sands into fertile land using $CO_2$ adsorbed on clays, offering a novel solution to combat desertification and mitigate climate change. We developed $CO_2$-enriched fertilizers using the solgel method, and the process involved purifying raw kaolinite followed by CTAB intercalation and impregnation with varying concentrations of polyethyleneimine (PEI) (30 and 50%). The prepared fertilizers were analyzed using FTIR, XRD, SEM, and TEM to assess their structural and morphological properties. Furthermore, these adsorbents were evaluated for $CO_2$ uptake potential. The highest $CO_2$ adsorption capacity of 167.1 mg $g^{-1}$ was obtained with CKP-50 much higher than unmodified kaolinite (0.901 mg $g^{-1}$). FTIR analysis confirmed that $CO_2$ adsorption on the prepared fertilizers occurred *via* chemical interaction with amine groups. The $CO_2$-enriched clays were mixed with sand in appropriate concentrations to support plant growth in desert lands. The plant growth trial showed significant improvements with PEI impregnated samples, S-CKP-30 and S-CKP-50, which supported taller and healthier plants compared to pure kaolinite (S-PK) and CTAB-modified kaolinite (S-CKP-0). By day 30, plants with S-CKP-50 reached 27.1 cm in height demonstrating enhanced plant growth, especially in arid conditions, by improving moisture retention, nutrient availability, and increased $CO_2$ adsorption. These results showed that our prepared fertilizers, especially S-CKP-50, proved to be the most effective material for $CO_2$ mitigation and promoting plant growth, hence offering a promising approach to desert reclamation and $CO_2$ sequestration simultaneously.

Received 15th December 2024,
Accepted 2nd April 2025

DOI: 10.1039/d4ma01246a

rsc.li/materials-advances



## 1. Introduction

Elevated carbon dioxide ($CO_2$) concentrations contribute to climate change, global warming, and extreme weather events. $CO_2$ levels above 4% can also harm human health, causing fatigue, headaches, and asphyxiation risks.[1] To address this, carbon capture and utilization (CCU) technologies are being developed to capture $CO_2$ emissions from industrial processes and power generation.[2] These include post-combustion capture, pre-combustion capture, and direct air capture (DAC),[3] with $CO_2$ being utilized in applications such as enhanced oil recovery (EOR), the production of synthetic fuels, chemicals, and building materials, and even in agricultural practices like enhancing soil fertility. These technologies help to reduce atmospheric $CO_2$ levels, mitigate health risks, and contribute to global climate change efforts.[4,5]

Desertification is one of the most pressing environmental challenges faced by the world today, with vast areas of the Earth's surface increasingly becoming barren and unproductive.[6,7] Land degradation threatens livelihoods, with 20 million hectares lost yearly, potentially reducing global food production by 12%.[8] One-third of agricultural land has become barren in the last 40 years. Degraded soil reduces crop productivity, and global food production could drop by 12% in the next 25 years, raising food prices by 30%. The annual cost of land degradation is 3.4 trillion euros, driven by factors like population growth, biofuel demand, poverty, and climate change. In sub-Saharan Africa, 50% of agricultural land has lost productivity, and 80% of rangelands show signs of degradation. Globally, 56% of degraded land results

[a] *Interdisciplinary Research Center for Hydrogen and Energy Storage (IRC-HES), King Fahd University of Petroleum & Minerals (KFUPM), Dhahran 31261, Saudi Arabia. E-mail: safyan@kfupm.edu.sa*
[b] *School of Material Science and Engineering, Henan University of Technology, Zhengzhou 450001, Henan, China*

† Electronic supplementary information (ESI) available. See DOI: https://doi.org/10.1039/d4ma01246a

from water erosion, 28% from wind erosion, and 12% from chemical degradation. About 3.6 million hectares of drylands are at risk of degradation.[8] The loss of soil fertility is particularly critical in desert regions, where natural conditions already limit agricultural productivity.

Conventional methods such as irrigation and chemical fertilizers[9] have been used to address these issues, but they are often unsustainable in the long term due to resource constraints, high costs, and environmental harm.[10,11] Additionally, traditional fertilizers often lead to nutrient imbalances in the soil, negatively affecting microbial communities and overall soil health.[12,13] Overuse can lead to soil degradation, depletion of essential minerals, water pollution,[14,15] health risks (blue baby syndrome, cancer *etc.*),[16] greenhouse gas emissions, and contamination with heavy metals (as seen in the Gulf of Mexico's "dead zone") and radionuclides like U238, Th232, and Po210.[17,18] Many studies have been conducted worldwide to analyze the side effects of conventional fertilizers;[19] for example, Abebe *et al.* discuss how Ethiopia's over-use of fertilizers has resulted in soil fertility depletion and low crop yields.[20] Long-term fertilizer use in India has led to increased heavy metal accumulation in soil, posing potential long-term risks to crop growth and environmental health.[21] Guo & Wang analyzed $NH_3$ emissions from synthetic nitrogen fertilizers in China from 1991 to 2013, showing an increase from 3.20 to 5.21 Tg $NH_3$ per year.[22] Another study identified excessive fertilizer and pesticide use in China (cities like Shandong and Qinghai) as a key factor contributing to total phosphorus loss, and driving water eutrophication.[23] Ghanem *et al.* examined how air and soil pollution affect social development in Saudi Arabia, showing that increased fertilizer and pesticide use, and $CO_2$ emissions raise hospitalizations.[24] Al-Busaidi *et al.* (1993–2020) found that long-term farming caused soil salinization, reduced pH, and elevated phosphorus and ion levels.[25] Sulaiman *et al.* analyzed toxic metals in fertilizers and their accumulation in soil and date palms in the UAE.[26] Al-Taani *et al.* analyzed heavy metal pollution in Liwa, UAE, finding Cd, Ni, Zn, and Cr enriched due to agrochemicals. The pollution load index indicated low to moderate contamination, with Cd posing a high ecological risk.[27] These worldwide studies show the requirement for alternative, eco-friendly fertilizers that provide essential nutrients without these negative consequences.

Traditionally seen as harmful to the environment, $CO_2$ can be captured and transformed into a beneficial substance.[28,29] $CO_2$ utilization is a growing area of research, with several innovative applications in different[30] fields, especially in agriculture, where $CO_2$ can be harnessed as a valuable resource to improve soil fertility, enhance crop yields, and combat desertification. By capturing $CO_2$ and using it to improve soil quality, particularly in arid regions like deserts, it is possible to transform infertile land into fertile, productive soil. One such method involves the adsorption of $CO_2$ onto adsorbents, a process that can provide long-term benefits for soil fertility.[31] Fig. 1(b) illustrates the possible interactions of $CO_2$ in the soil. $CO_2$ in soil undergoes several important chemical reactions that affect soil health and carbon cycling. When $CO_2$ enters soil moisture, it reacts with water to form carbonic acid ($H_2CO_3$), which helps in mineral weathering and nutrient release, such as calcium and magnesium. This acid dissociates into bicarbonate ($HCO_3^-$), which can alter soil pH and contribute to carbonate formation, effectively sequestering carbon. Soil microorganisms also play a vital role in converting organic carbon into stable soil organic matter (SOM), which improves soil fertility. In anaerobic conditions, some microbes transform $CO_2$ into methane ($CH_4$), while others release $CO_2$ during respiration. These processes are crucial for nutrient cycling, carbon sequestration, and overall soil health.

Various materials have been explored for their ability to effectively adsorb carbon dioxide ($CO_2$) due to their high surface area, porosity, and chemical properties, such as zeolites,[32,33] metal–organic frameworks (MOFs),[34,35] carbon nanotubes (CNTs)[36–38] metal oxides,[36,39] biochar,[40,41] carbon-based materials[42–45] and silica-based adsorbents.[46]

Clay minerals abundant in desert regions have long been recognized for their beneficial properties in soil enhancement. These minerals have a large surface area and high cation-exchange capacity, making them excellent candidates for improving soil structure, water retention, and nutrient availability.[47] The adsorption of $CO_2$ onto clay including kaolinite,[48] montmorillonite,[49] and bentonite[50] has been extensively studied in recent years due to their potential for carbon sequestration as well as soil enhancement. $CO_2$ adsorbed onto clay minerals forms stable complexes that release essential nutrients like potassium, calcium, and magnesium, improving soil fertility and structure. This process improves soil structure, boosts microbial activity, and increases cation-exchange capacity.

Kaolinite, a naturally abundant clay mineral, has been investigated as a potential adsorbent for $CO_2$ capture and storage applications. Kaolinite is a 1 : 1 layered aluminosilicate with a relatively low cost, high surface area, and chemical stability, making it an attractive candidate for adsorption-based $CO_2$ capture.[2,3] However, the native kaolinite exhibits very low $CO_2$ adsorption capacity, typically around 3 mg $CO_2$ per g or less under ambient conditions.[4,5] To improve its $CO_2$ adsorption performance various modification techniques are employed such as acid activation leading to enhanced $CO_2$ adsorption capacities of up to 3.4 mg $CO_2$ per g.[48] A study found that substituting Al in kaolinite with elements like Mn, Fe, Co, Ni, or Si enhances $CO_2$ adsorption by altering its electronic structure and surface properties, as shown by DFT calculations.[51] ZSM-5 molecular sieve was prepared from kaolin and modified with Na, Ni, and Ni–Na to create Ni–Na/ZSM-5 (1.5Ni–0.6Na), which exhibited the best $CO_2$ adsorption capacity of 1.97 mmol $g^{-1}$.[52] Kaolin-derived 4A-zeolite was modified with TEPA and DEA to optimize $CO_2$ adsorption. Optimal 4A-DEA achieved 579 mg $g^{-1}$ capacity.[53] Activated carbon (AC), kaolinite (KAO), and kaolinite-activated carbon composite (KAC) were evaluated as $CO_2$ adsorbents, with maximum capacities of 28.97 mg $CO_2$ per g for AC, 18.54 mg $CO_2$ per g for KAC, and 12.98 mg $CO_2$ per g for KAO.[54]

The cationic surfactant CTAB (cetyltrimethylammonium bromide) has been used to modify clays, introducing positively

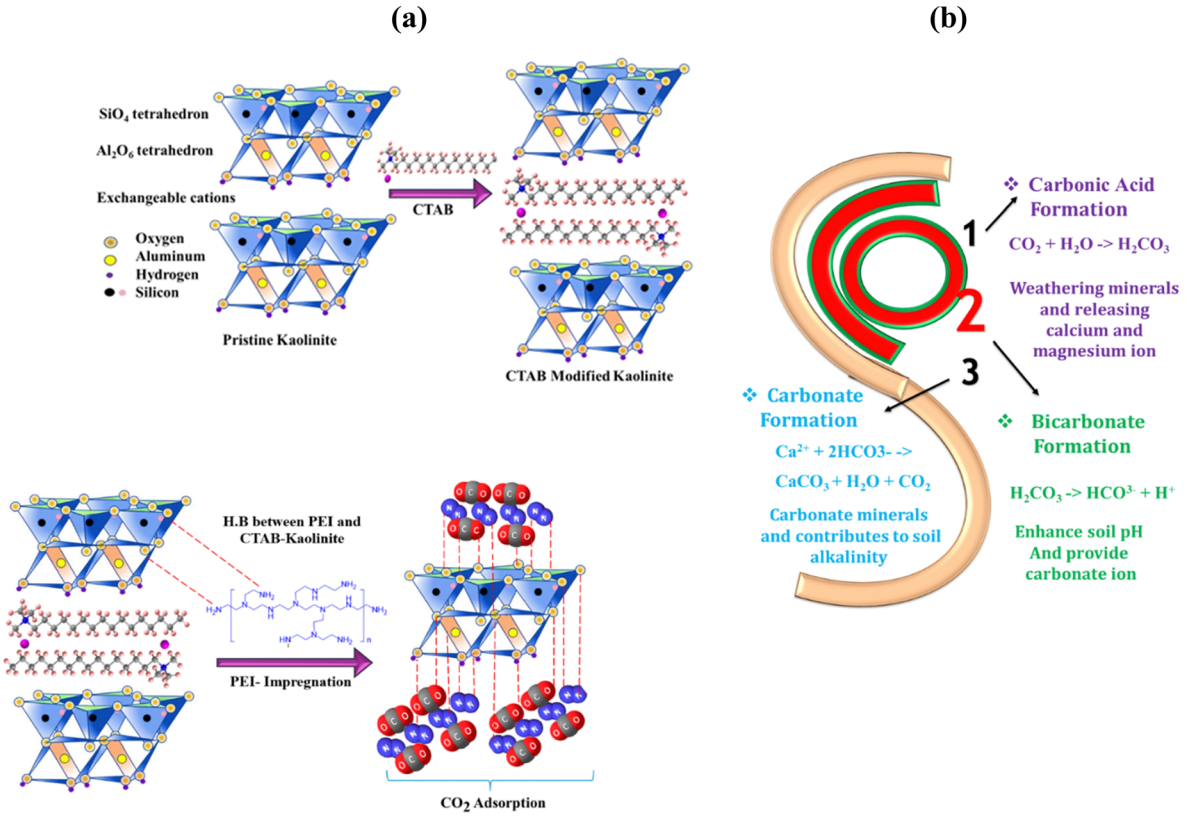


Fig. 1 (a) Synthesis of PEI-impregnated clay-based $CO_2$-enriched fertilizers, and (b) illustration of possible interactions of $CO_2$ in soil.

charged organic cations onto the surface, changing hypoploidy and surface charge.[55] Introducing amine functional groups onto the kaolinite surface can improve the affinity towards $CO_2$ through chemisorption. Amine modification significantly enhanced kaolinite's low native $CO_2$ adsorption capacity.[56] PEI (polyethyleneimine) enhances $CO_2$ adsorption in various solid adsorbents. For example, protonated titanate nanotubes (PTNTs) modified with 50 wt% PEI demonstrated a high $CO_2$ capacity of 130.8 mg $g^{-1}$ at 100 °C.[57] Similarly, a study examines $CO_2$ adsorption on polyethyleneimine (PEI) loaded onto porous carbon (PC) with varying pore sizes. The highest $CO_2$ adsorption was observed in PC with a 3.63 nm pore size at 50 °C.[58]

Desert sand presents significant challenges for plant growth due to nutrient deficiency, poor water retention, and unfavorable soil structure. To overcome these issues, this study aimed to develop and evaluate $CO_2$-based fertilizers as a solution to enhance desert soils. These fertilizers can improve soil fertility, enhance water retention, and promote better soil structure by reducing compaction and balancing pH. Additionally, they contribute to carbon sequestration, which helps mitigate climate change. The study hypothesized that $CO_2$-based fertilizers would not only enhance desert soil health but also promote resilient agriculture in arid regions. To test this, kaolinite clay was selected, modified with CTAB, and impregnated with PEI. The materials were characterized using XRD, BET, FTIR, SEM, and TEM. $CO_2$ adsorption capacity was evaluated for each sample, and the $CO_2$-enriched fertilizers were mixed with desert sand to assess their impact on plant growth in a controlled trial. The study's objective was to demonstrate that low concentrations of these fertilizers can improve soil fertility, water retention, and structure without disrupting the desert ecosystem, offering a sustainable solution for agriculture and ecological restoration in arid regions.

## 2. Materials and methods

The raw kaolinite was purchased from Fluka. The hydrochloric acid (HCl, 36%), sodium chloride (NaCl, 60%), sodium hydroxide (NaOH, 97%), cetyltrimethylammonium bromide (CTAB), polyethyleneimine (PEI), toluene, and methanol (MeOH) were used for the purification and modification of kaolinite and purchased from Sigma Aldrich. Distilled water was used throughout the experiment.

### 2.1. Preparation of $CO_2$ enriched fertilizer

Herein we developed a nanocomposite adsorbent for dual function purposes by employing a solgel method. This technique involves the transition of a liquid precursor into a gel-like network, which is then heated to form a solid material. It is widely used for producing highly uniform materials with specific properties, such as high surface area and porosity. In the context of this study, the sol–gel method was used to modify kaolinite by incorporating surfactants (CTAB) and amines (PEI),

enhancing its $CO_2$ adsorption capacity and improving its potential for soil modification. This process allows for precise control over the material's chemical structure and properties, making it ideal for creating $CO_2$-enriched fertilizers. The schematic for the synthesis of CTAB-modified kaolinite impregnated with PEI fertilizers and the $CO_2$ adsorption process is depicted in Fig. 1(b), and a detailed description is given as:

• Purification of kaolinite: the purification of kaolinite using water, also known as beneficiation, is a crucial process for enhancing the quality of kaolin clay. This method primarily relies on physical separation techniques to remove impurities and improve the clay's properties. Initially, 10 grams of raw kaolinite (Kao) were dispersed in 1000 mL of deionized water to ensure the complete distribution of the clay in the aqueous medium followed by stirring for 24 hours to ensure the complete and uniform distribution of the kaolinite throughout the aqueous medium. After stirring, the resulting suspension was filtered to separate the purified kaolinite from any coarse particles or contaminants. The filtered clay was then subjected to vacuum drying at 100 °C, which removed the water content and left behind a dry, powdery form of kaolinite. The purified kaolinite, free from impurities, was subsequently coded as ''PK'' and is now ready for further modification or use in various applications. This method effectively produces a clean and homogeneous kaolin sample suitable for advanced use.

• CTAB intercalation: the synthesis of cetyltrimethylammonium bromide (CTAB) modified kaolinite was conducted using a specific procedure. The process began by dispersing 1 g of pure kaolinite (PK) in 100 ml of distilled water. This mixture was then stirred using a magnetic stirrer for 24 hours at room temperature. The purpose of this step was to allow the kaolinite to swell and reach a homogeneous state. After the dispersion and swelling process, the desired amount of CTAB was slowly added to the dispersed PK. The amount of CTAB used was equivalent to 1.0 times the cation exchange capacity (CEC) of the kaolinite. Following the addition of CTAB, the reaction mixture was stirred for 5 hours. This stirring facilitated the interaction between the CTAB and the kaolinite, resulting in the formation of the CTAB-modified kaolinite, also known as organoclay. Once the stirring was complete, the resultant organoclay was filtered. The filtered organoclay was then washed with distilled water several times to remove any excess salts that may have been present. After the washing step, the organoclay was dried in an oven at a temperature of 90 °C. Finally, the dried organoclay was ground and sieved using standard sieves to obtain the chemically modified adsorbent material. This comprehensive procedure ensured the successful synthesis of CTAB-modified kaolinite (CK or CKP-0), which can be used as an effective adsorbent material for various applications.

• PEI-modification: the exfoliation technique was employed to attach amine groups to the surface of CTAB-intercalated kaolinite. The synthesis of polyethyleneimine (PEI)-impregnated CK was carried out using 30% and 50% wt PEI loadings. The process began by preparing a PEI solution in a 100 mL round-bottom flask, where the measured amount of PEI was dissolved in 40 mL of methanol (MeOH) and the solution was then stirred at room temperature for 30 minutes to ensure complete dissolution of the PEI.

In a separate beaker, approximately 0.5 g of CTAB-modified kaolinite (CK) was added into 5 mL of toluene. The mixture was sonicated in an ultrasonic bath for 5 hours at room temperature. Once prepared, the CK solution was added to the previously prepared PEI solution. The mixture was then stirred for an additional 3 hours to facilitate the interaction between the PEI and the CTAB-modified kaolinite (CK), allowing the PEI to be effectively incorporated onto the surface of the CK. Once stirring was completed, the stir bar was removed, and the clay was allowed to settle at the bottom of the flask. The methanol layer on top was decanted, and the wet clay was dried in a vacuum oven at 75 °C for 12 hours. This procedure was repeated with increasing concentrations of PEI, resulting in two adsorbents (CKP-30 and CKP-50, which refer to CTAB-modified kaolinite samples with 30% and 50% PEI, respectively). The resulting CKP clay materials were characterized using several analytical techniques, including FTIR, EDX, and TEM, providing detailed information on the properties and composition of the PEI-treated CK. Table S1 (ESI†) shows the code and composition of the prepared samples. The percentage yield for each step was calculated and given in the ESI.†

# 3. Characterization techniques

## 3.1. Fourier transform infrared spectroscopy (FTIR)

Fourier-transform infrared (FTIR) analysis is a valuable procedure used to investigate the chemical composition and molecular structure of materials. The FTIR of all prepared samples was carried out using a Nicolet 550, to identify the structural changes after CTAB interaction in kaolinite and PEI impregnation. The FTIR spectra were recorded by directly contacting the samples with an ATR (attenuated total reflectance) tip and spectra were obtained by conducting 64 scans in the range of 4000–400 $cm^{-1}$.

## 3.2. X-Ray diffractometer (XRD)

The crystallography of the synthesized samples was investigated through X-ray diffraction (XRD) analysis. The XRD patterns were attained at room temperature using an X-ray powder diffractometer, specifically a D/Max-3A Rigaku, with Cu Kα radiation ($\lambda$ = 1.5418 Å), a voltage of 35 kV, and a current of 30 mA. The data was obtained over an angular range from 0 to 100° in increments of 0.02°, employing an X-ray generator.

## 3.3. Scanning electron microscopy (SEM)

Scanning electron microscopy (SEM) was used to characterize surface morphologies of all prepared samples. The LEO 1530 scanning electron microscope, USA, is utilized for this purpose. The instrument is coupled with an energy dispersive X-ray spectrometer (EDS) detector to facilitate elemental analysis. The spatial resolution of the detected elements is contingent on the energy of the primary electron beam, the atomic number of the constituent elements, and the sample material's

thickness. SEM provides high-resolution images, while EDS enables the identification and quantification of elements present in the samples, including mapping the spatial distribution of elements across the surfaces. This comprehensive analysis aids in understanding the structural and elemental properties crucial for optimizing the performance of these composite membranes.

### 3.4. Field emission transmission electron microscope (FETEM)

The field emission transmission electron microscope (FETEM) is a multipurpose, 200 kV FE (field emission) analytical electron microscope that was used to analyze all prepared samples; pure kaolinite (PK), CTAB modified kaolinite (CK or CKP-0), CTAB modified kaolinite with 30 and 50% PEI (CKP-30, CKP-50).

### 3.5. Brunauer–Emmett–Teller (BET)

The surface area and total pore volume of all prepared fertilizers were determined using a Quantachrome QuadraWin (version 6.0) instrument through nitrogen adsorption at liquid nitrogen temperature. Sample preparation involved degassing overnight for 2 hours at 130 °C under vacuum. The Brunauer–Emmett–Teller (BET) method was employed. This analysis provides precise evaluation of specific surface area through nitrogen multilayer adsorption measured as a function of relative pressure. The BET method allows for the determination of surface area in $m^2\ g^{-1}$, offering valuable insights into surface porosity.

## 4. Results and discussion

### 4.1. Fourier transform infrared spectroscopy (FTIR)

Infrared spectroscopy is used to identify the presence of organic molecules within the clay layers. To confirm the intercalation of quaternary alkylammonium cations into the silicate structure, FTIR spectra of pure kaolinite (PK) and CTAB-modified kaolinite (CKP-O) were recorded and compared. From Fig. 2, PK shows four characteristic OH-stretching bands,[59] the band at 3698 relates to inner-surface OH in-phase stretching, those at 3671 and 3655 $cm^{-1}$ are inner-surface OH anti-phase stretching and that at 3621 $cm^{-1}$ is due to the stretching of inner stretching OH groups.[60–62] In CKP-0, peaks at 2860 $cm^{-1}$ and 2981 $cm^{-1}$ correspond to the symmetric and asymmetric stretching vibrations of the methyl ($CH_3$) and methylene ($CH_2$) groups from the aliphatic chain of the surfactant, with these peaks appearing more prominently[63] in CKP-0. The presence of these peaks indicates the incorporation of surfactants into PK. The other typical absorption bands of PK at 3667 $cm^{-1}$ and 3607 $cm^{-1}$ are attributed to the inner OH groups bonded to Al or O. The stretching peak at 908 $cm^{-1}$ is associated with the Si–O or Si–O–Al bonds.[60] The peak observed at 1394 $cm^{-1}$ corresponds to the C–N group of the organic modifier, confirming the intercalation of surfactant molecules between the silicates. The characteristic bands of the C–N bond, typically found between 910 and 1000 $cm^{-1}$ (particularly strong for compounds like R–N + $(CH_3)_3$), are obscured in the complex inorganic-clay structure due to the deformation vibrations of Al–OH at 926 $cm^{-1}$.[64]

In the spectra of PEI-based composite adsorbents (CKP-30 and CKP-50), the bands at 2850 and 2925 $cm^{-1}$ can be attributed to the stretching vibrations of $-CH_2$ groups in the PEI chain.[65] Two bands at 1590 and 1447 $cm^{-1}$ are attributed to the symmetric and asymmetric bending vibrations of $-NH_2$, while another band at 1660 $cm^{-1}$ corresponds to the bending vibration of –N(R)H in PEI. Notably, as the PEI loading increased, the intensity of these bands grew, indicating that more PEI was dispersed inside the pores and/or on the inner surface of PK. Additionally, these peaks showed a slight shift from their original positions, suggesting a weak interaction between PEI and the internal surface of the clay.

### 4.2. X-Ray diffraction (XRD)

Fig. 3 shows the XRD pattern of PK, CKP-0, CKP-30 and CKP50. The structure of pure kaolinite (PK) before and after modification with CTAB was compared, for PK, the peaks at 12.18°, 20.2°, 21.23°, 23.3°, 24.78°, 35.89°, 38.83°, and 55.99° can be

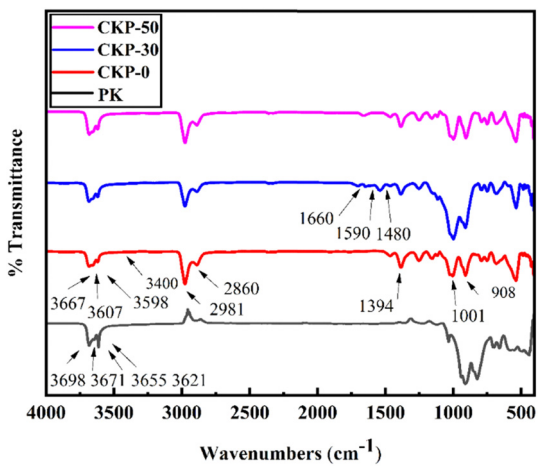


Fig. 2 The FTIR spectra of PK, CKP-0, CKP-30 and CKP50.

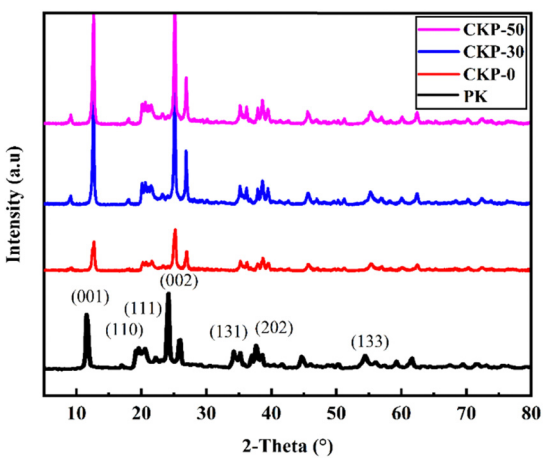


Fig. 3 XRD pattern of PK, CKP-0, CKP-30 and CKP50.

indexed to the planes corresponding to kaolinite (001), (110), (111), (002), (131), (202), and (133), respectively.[66,67] In the case of CKP-0, the characteristic (001) diffraction peak of PK shifts from 12.1895° to 12.2721° after treatment with CTAB, indicating the intercalation of CTAB into the kaolinite layers. The *d*-spacing of kaolinite at (001) increases from 7.13411 to 7.15163 Å, further supporting the intercalation of CTAB. The addition of the surfactant increases the basal spacing of the resulting organoclay, suggesting the placement of $CTA^+$ ions between the clay layers and leading to a decrease in hydration water content. As a result, the surface properties change from hydrophilic to hydrophobic.[64] XRD analysis was also conducted to examine the impregnation of PEI into CTAB modified kaolinite. The results showed an increase in *d*-spacing in the CKP composites from 1.36 to 1.92 nm after reaction with PEI, indicating the successful synthesis of intercalated PEI nanocomposites.

### 4.3. Transmission electron microscopy (TEM)

Transmission electron microscopy (TEM) images of pure kaolinite (PK) in Fig. 4(a) reveal its characteristic morphology, typically appearing as hexagonal or pseudo-hexagonal platelets. These platelets can be observed in both face-on and edge-on orientations, providing insights into the mineral's structural arrangement. These images also highlight the stacking order of the layers, where well-ordered PK shows regular, parallel fringes, while disordered samples may exhibit wavy or discontinuous patterns. Additionally, TEM analysis reveals structural defects like stacking faults and intergrowths with other clay minerals. TEM images of CTAB-modified kaolinite, *i.e.* CKP-0 (Fig. 4(b)), reveal significant structural changes and enhanced properties resulting from the modification process. The images show successful intercalation of CTAB molecules into the interlayer spacing of PK, leading to a slight expansion of the basal spacing. Despite this modification, the characteristic hexagonal or pseudo-hexagonal platelet structure of PK is preserved, indicating that its inherent properties remain intact. TEM analysis also demonstrates a homogeneous distribution of CTAB throughout the PK material, contributing to a more porous surface morphology that enhances adsorption capabilities. Additionally, the modification significantly reduces particle agglomeration compared to unmodified kaolinite. It is worth noticing that the structural integrity of kaolinite is maintained during the modification process.[68]

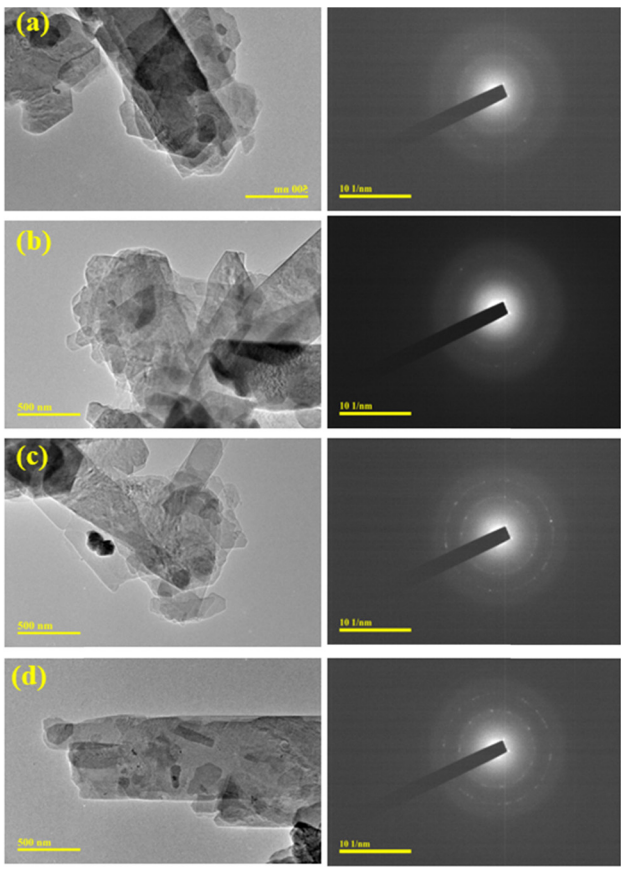


Fig. 4 TEM images of (a) PK, (b) CKP-0, (c) CKP-30 and (d) CKP50.

TEM photographs of PEI-impregnated CTB modified kaolinite with 30 and 50% PEI loading (CKP-30 and CKP-50) presented in Fig. 4(c) and (d) showed that PEI is impregnated homogeneously into the clay layers on the nanoscale, although some particles of clay were agglomerated. As polyethyleneimine (PEI) loading increased, the intercalation of PEI molecules between the clay sheets also increased, hence leading to greater adhesion with the clay layers, resulting in a more complex structure. Such interactions improve various properties of the resulting nanocomposites, such as mechanical strength, thermal stability, and gas barrier properties.[69]

### 4.4. Scanning electron microscopy (SEM)

SEM analysis was conducted to assess the surface morphology of both pure and modified kaolinite clays, with the results shown in Fig. 5. The surface morphologies of pure kaolinite (PK) and CTAB-modified kaolinite (CKP-0) differ significantly. The PK surface is characterized by stacked pseudo-hexagonal platelets with diameters ranging from 0.1 to 1.5 μm and thicknesses of approximately 30–100 nm (Fig. 5(a)). These platelets form "booklet" structures several micrometers in size, especially noticeable in CKP-0, where a high degree of stacking exposes the edge surfaces. Both PK and CKP-0 have uneven structures with non-uniform size distributions, with kaolinite displaying a more aggregated morphology and occasional large flakes. After modification, the surface of PK was transformed into a non-aggregated morphology, featuring numerous small, crumpled flakes. Additionally, the surface of CKP-0 expanded due to the chemical intercalation of CTAB. The expanded interlayer created by the CTAB modification of kaolinite provides a favourable site for chemical reactions such as interlayer exchange and adsorption. It has been shown that CTAB-modified kaolinite has a larger pore size compared to PK (Fig. 5(b)).

SEM images of the PEI/CTAB-kaolinite composites (CKP30 and CKP50) reveal minimal PEI on the external surfaces, suggesting that the PEI is dispersed within the pores of the

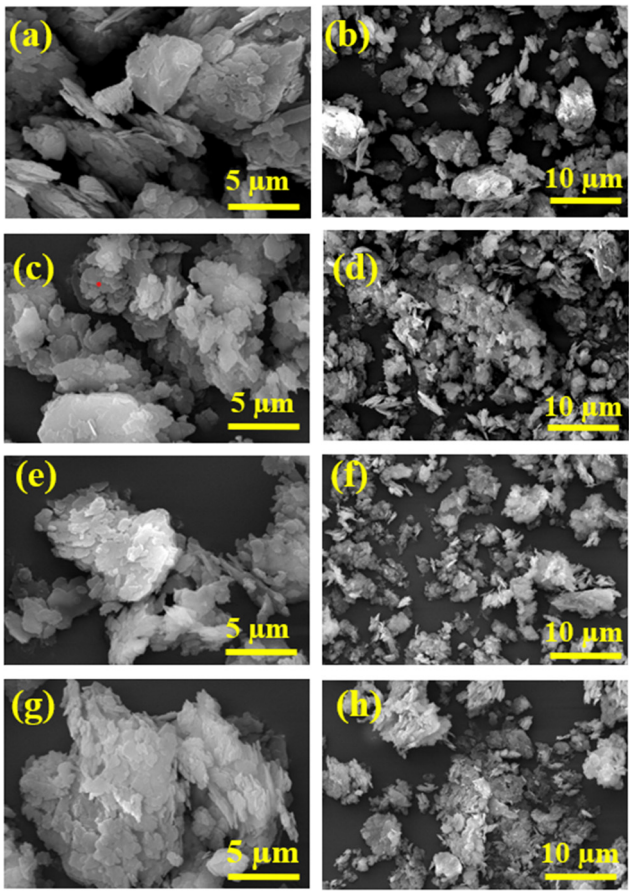


Fig. 5 SEM images of (a) and (b) PK, (c) and (d) CKP-0, (e) and (f) CKP-30 and (g) and (h) CKP50.

CTAB-modified kaolinite (Fig. 5(c) and (d)). The images indicate excellent adhesion between the CTAB-kaolinite particles and the PEI polymer matrix, with no voids observed, likely due to the high compatibility between the particles and the polymer, which is facilitated by ammonium ion treatment. For CKP30 (30 wt% PEI), only a small amount of PEI was observed on the external surfaces, while some PEI was coated on the clay particles, leading to partial agglomeration. At PEI loadings below 50 wt%, most of the PEI was found within the pores of the samples.

For CKP50, which had a higher PEI loading (50 wt%), a significant portion of the PEI was present on the external surfaces, acting as linkages between the clay particles. The amine groups in PEI likely bond with the Si–OH and Al–OH groups on the surface of the modified kaolinite, increasing the PEI loading. Based on the SEM observations, it was found that composites with PEI content up to 50 wt% remained as powders. These findings suggest that the optimal PEI loading for preparing effective composite sorbents is approximately 50 wt%, which aligns with the observed $CO_2$ sorption capacity trends of the sorbents at different loadings.

### 4.5. Energy dispersive spectroscopy (EDS)

The EDS analysis of PK, CKP-0, CKP-30 and CKP-50 provides important insights into the elemental makeup of these materials. In the case of PK, the EDX spectrum typically reveals dominant peaks for silicon (Si), aluminum (Al), and oxygen (O), which are the key elements that make up the clay mineral. These elements are representative of kaolinite's characteristic layered silicate structure (Fig. 6(a)). Upon modification with cetyltrimethylammonium bromide (CTAB), the EDX spectrum of CKP-0 would display additional peaks for carbon (C), nitrogen (N), and bromine (Br). The presence of these elements confirms the successful incorporation of CTAB into the kaolinite structure, which enhances the material's properties for a range of applications. The carbon peak is particularly notable, as it corresponds to the alkyl chains in CTAB, while the nitrogen and bromine peaks are associated with the ammonium group and bromide ion, respectively (Fig. 6(b)). For the PEI-impregnated samples (CKP-30 and CKP-50), EDX analysis would show stronger carbon and nitrogen peaks compared to the CTAB-modified kaolinite. This increase is due to the inclusion of polyethyleneimine (PEI), which has a high content of carbon and nitrogen due to its polymeric structure. The intensity of these peaks would be more pronounced in the 50 wt% sample compared to the 30 wt% sample, indicating a higher amount of PEI loading in the former (Fig. 6(c) and (d)).

In summary, EDX analysis is a valuable technique for verifying the successful modification of kaolinite with CTAB and PEI. It provides quantitative data on the elemental composition of the nanocomposite materials, which correlates with their enhanced properties.

### 4.6. Brunauer–Emmett–Teller (BET)

Table 1 presents the BET surface area, and total pore volume of PK, CKP-0, CKP-30, and CKP-50. The analysis showed that the total surface area of kaolin clay significantly decreased from 20.57 to 5.03 $m^2\ g^{-1}$ after modification with the CTAB surfactant. In contrast, the total pore volume increased from 0.305 to 0.591 $cm^3\ g^{-1}$ and pore diameter 9.75 to 21.09 nm. These results align with previous studies on surfactant-modified clays.[70,71] The reduction in surface area, along with the increase in pore volume and pore diameter can be attributed to the intercalation of surfactants, which filled much of the gallery space in the clay, causing the interlayer to expand and thus increasing the pore volume. For the CKP-30 and CKP-50 samples, the surface areas were 3.97 and 3.31 $m^2\ g^{-1}$ and the pore volume was 0.06 and 0.04 $cm^3\ g^{-1}$, respectively, while the pore diameter was 23.09 and 23.15 nm, respectively, after the introduction of PEI into the CTAB-modified kaolinite.

The amount of $N_2$ adsorption and pore volume decreased with increasing PEI loading, as the PEI filled the pores and channels between the clay layers. This led to a reduction in pore volume with increasing PEI content. It can be observed that the amine impregnated sample has a lower surface area and pore volume. This is because amine molecules entered the surface pores of the kaolinite and blocked them, thereby reducing the textural properties of the amine-loaded CK sample. The surface area of the CKP-30 sample (with 30% PEI loadings) decreased to 3.39 $m^2\ g^{-1}$, and the pore volume also diminished, and a

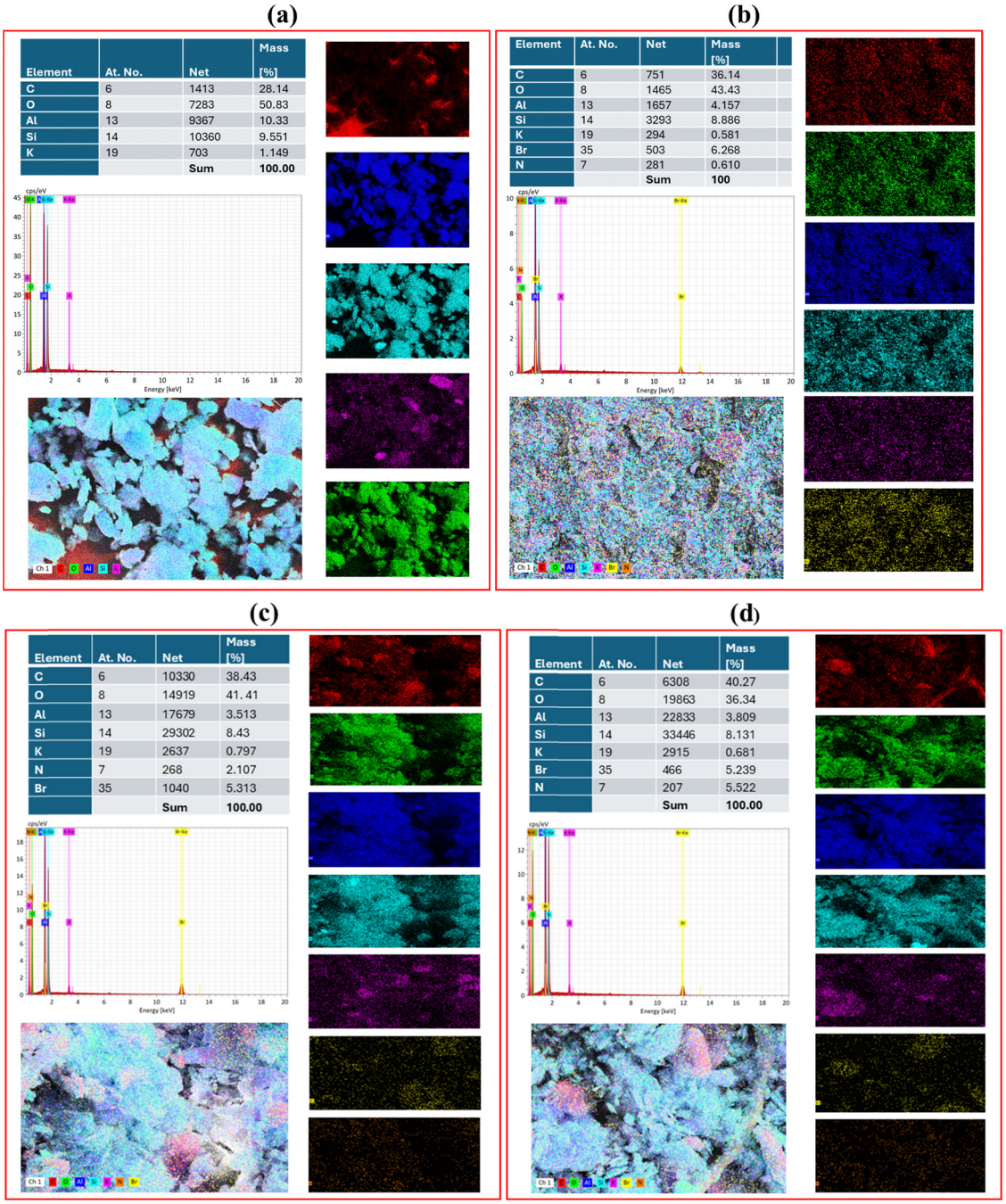


Fig. 6 EDX and elemental mapping of (a) PK, (b) CKP-0, (c) CKP-30, and (d) CKP-50.

Table 1 Summary of BET surface area, pore volume, and $CO_2$ uptake for PK, CKP-0, CKP-30, and CKP-50

| Samples | BET surface area ($m^2\ g^{-1}$) | Total pore volume ($cm^3\ g^{-1}$) | $CO_2$ capacity ($mg\ g^{-1}$) |
|---|---|---|---|
| PK | 20.57 | 0.305 | 0.901 |
| CKP-0 | 5.03 | 0.591 | 3.44 |
| CKP-30 | 3.97 | 0.06 | 150.0 |
| CKP-50 | 3.31 | 0.04 | 167.1 |

further increase up to 50% PEI loading led to the filling of the pores and channels in the CK layers and caused further reduction in these surface feature. These results are in agreement with the SEM and TEM findings.

The CKP-50 sample exhibited the highest $CO_2$ adsorption capacity compared to the other samples (Table 1). This suggests that the $CO_2$ adsorption capacity improves with higher amine loading. The increase in capacity is attributed to the interaction between amine groups and $CO_2$ molecules. A higher weight ratio of amines results in more amine groups being incorporated, thereby enhancing the material's adsorption capability. Interestingly, the $CO_2$ adsorption capacity did not correlate directly with the BET surface area or pore volume, suggesting

that these factors were not the primary contributors to the $CO_2$ adsorption performance. Instead, the amount of PEI loading and the availability of reaction sites on the adsorbent played a more significant role. While an optimal amount of PEI is necessary, excessive PEI loading can block the internal and inter-particle pores of the sample, potentially decreasing $CO_2$ uptake.[72] Based on the results, the optimal PEI loading in the current study was maintained in the range of 50–60 wt%.

### 4.7. $CO_2$ uptake study

The $CO_2$ adsorption experiments were conducted at 298 K using ultra-high pure $CO_2$ (99.99%) gas with a 20 mL $min^{-1}$ flow rate. The PK sample has low $CO_2$ uptake due to several structural and chemical limitations. Its specific surface area is high, but it has no fictional groups that can chemically bind $CO_2$, which restricts the available sites for $CO_2$ adsorption. Additionally, kaolinite has a minimal pore volume of about 0.035 cc $g^{-1}$ and lacks a microporous structure, leading to adsorption primarily on particle surfaces and in larger macropores. The weak interactions between $CO_2$ and the –OH groups on its surface further limit its capacity. Moreover, the tight layered structure of kaolinite prevents $CO_2$ from intercalating between the layers. As a result, the $CO_2$ adsorption capacity of raw kaolinite is extremely low, making it ineffective for $CO_2$ capture applications.

The chemical structure of cetyltrimethylammonium bromide (CTAB), a cationic surfactant, significantly influences its interaction with kaolinite clay. CTAB consists of a long hydrophobic alkyl chain (a cetyl group) and a positively charged quaternary ammonium head. This unique structure allows CTAB to interact effectively with the negatively charged surfaces of clay. When CTAB is introduced to a suspension of kaolinite, the hydrophobic tail of CTAB tends to adsorb onto the clay surface, while the positively charged head group interacts with the negatively charged sites on the kaolinite. This interaction leads to a reduction in the surface tension and increases the hydrophobicity of the clay particles.

Hydrophobic modification can improve the interaction between clay and $CO_2$, as the more hydrophobic surface can better accommodate non-polar molecules like $CO_2$. CTAB forms organoclays, which have unique properties compared to their unmodified counterparts. These organoclays can have improved pore volume for enhanced $CO_2$ adsorption. The structural changes induced by CTAB can lead to a more favorable arrangement for $CO_2$ molecules to be trapped within the clay matrix. The presence of CTAB can enhance the physical and chemical adsorption mechanisms of $CO_2$ on the clay surface. The positively charged ammonium groups in CTAB can interact with the electron-rich regions of $CO_2$, promoting chemisorption. Additionally, the increased surface area and porosity allow for greater physisorption of $CO_2$ molecules.

Polyethyleneimine (PEI) significantly enhances the ability of kaolinite to adsorb $CO_2$ through several mechanisms related to its chemical structure and properties. PEI is a branched polyamine that contains multiple amine functional groups, which play a crucial role in the adsorption process. When PEI is incorporated into CTAB-modified kaolinite, it increases the number of active sites available for $CO_2$ interaction, thereby improving the overall adsorption capacity. The primary mechanism by which PEI aids in $CO_2$ adsorption is through chemical interaction. The amine groups in PEI can react with $CO_2$ to form carbamate species, which enhances the binding of $CO_2$ to the kaolinite surface. This reaction occurs primarily at the primary and secondary amine sites of PEI, allowing for the effective capture of $CO_2$ molecules from the surrounding environment. Additionally, the incorporation of PEI into kaolinite modifies the surface properties of the clay. This modification can increase the hydrophilicity of the kaolinite, which helps in the formation of bicarbonate ions in the presence of moisture, further facilitating $CO_2$ capture. The presence of water can enhance the adsorption process as it promotes the formation of bicarbonate through the reaction of $CO_2$ with hydroxyl ions, which can be generated from the interaction of water with the amine groups of PEI. Moreover, the loading percentage of PEI is a critical factor influencing $CO_2$ adsorption performance. Optimal amine loading ensures that there are sufficient active sites for $CO_2$ interaction without causing steric hindrance that could reduce accessibility.

The CKP-50 sample exhibited the highest $CO_2$ adsorption capacity compared to the other samples (Table 1). Interestingly, the $CO_2$ adsorption capacity did not correlate directly with the BET surface area or pore volume, suggesting that these factors were not the primary contributors to the $CO_2$ adsorption performance. Instead, the amount of PEI loading and the availability of reaction sites on the adsorbent played a more significant role. While an optimal amount of PEI is necessary, excessive PEI loading can block the internal and inter-particle pores of the sample, potentially decreasing $CO_2$ uptake.[72]

The PEI-impregnated approach significantly enhances the $CO_2$ adsorption capacity of various solid adsorbents. Generally, higher amine loading results in an increased $CO_2$ adsorption capacity, as the incorporation of PEI introduces more active sites, facilitating $CO_2$ adsorption onto the solid adsorbent surfaces. For example, Cheng *et al.* studied the effect of amine loading (20–60 wt%) on Zn/Co zeolitic imidazolate frameworks (Zn/Co ZIFs) under pure $CO_2$ gas flow. They found that a 20% PEI loading increased the $CO_2$ adsorption capacity from 1.07 mmol $g^{-1}$ to 1.27 mmol $g^{-1}$, and it continued to rise up to 1.82 mmol $g^{-1}$ at 40 wt%. However, when the PEI loading was further increased to 60 wt%, the $CO_2$ uptake capacity decreased to 1.35 mmol $g^{-1}$. This reduction was likely due to the excess PEI blocking the main active sites on the adsorbent.[73] Based on these findings, it can be concluded that excessive amine content negatively impacts the $CO_2$ uptake capacity and adsorption rate of PEI-modified adsorbents. This is due to the increased resistance to $CO_2$ diffusion from thicker PEI layers at high amine loadings. Additionally, excess PEI can the block pores completely, reducing the surface area and pore volume, and decreasing the availability of effective active sites on the adsorbent. Therefore, identifying the optimal amine loading for a given support material is essential to maximize $CO_2$ adsorption. Taking these factors into account, the 30 wt% and 50 wt% PEI loadings were chosen in the current study to achieve the highest $CO_2$ adsorption capacity. The accumulation of $CO_2$ onto the amine-modified kaolinites may be

 

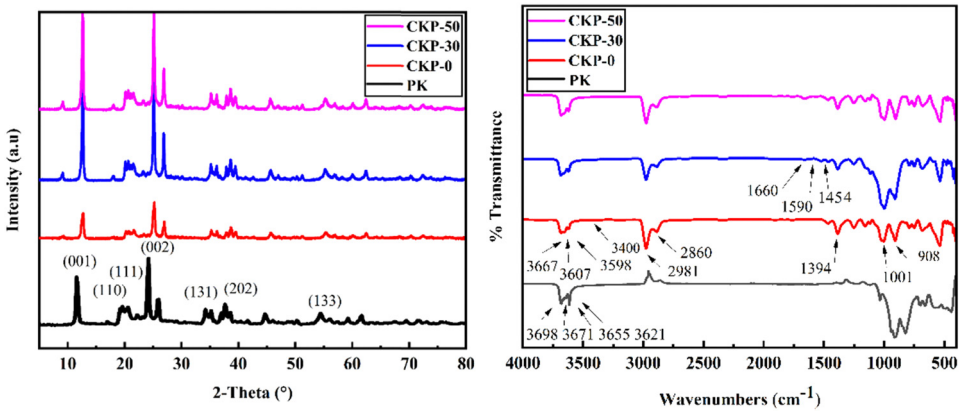


Fig. 7 FTIR and XRD analysis of all prepared fertilizers after the $CO_2$ adsorption study.

through chemical adsorption. The possible adsorption mechanism is in agreement with previous studies.[31,32]

**4.7.1. Resultant analyses after $CO_2$ adsorption.** The X-ray diffraction (XRD) pattern of amine-modified kaolinite (Fig. 7(a)) remains unchanged after $CO_2$ adsorption, with no new diffraction peaks appearing. Typically, if $CO_2$ molecules were to enter the interlayer space of kaolinite, the *d*-spacing (001) would increase. However, the position of the (001) peak does not shift, indicating that the spacing between the interlayers remains nearly the same. This suggests that very few, if any, $CO_2$ molecules are present within the interlayers, explaining why no noticeable change in spacing is observed.

The FTIR spectrum of the PEI impregnated CK after $CO_2$ adsorption, shown in Fig. 7(b), reveals a decrease or disappearance of the $NH_2$ bending bands at 1568 $cm^{-1}$ and 1490 $cm^{-1}$, as well as the $CH_2$ stretching modes at 2947 $cm^{-1}$ and 2870 $cm^{-1}$. Additionally, a new absorption peak appears at 1456 $cm^{-1}$, corresponding to the C–N vibration band, and another new peak appears at 1636 $cm^{-1}$, attributed to the $RNHCOO^-$ (carbamate species). These changes suggest a chemical reaction between the amine groups and $CO_2$ molecules, implying that $CO_2$ accumulation on the amine-modified kaolinites likely occurs through chemical adsorption. The adsorption mechanism is consistent with the findings of Gray *et al.* and Wang *et al.*

$$\text{Si–OH(kaolinite)} + \text{RNH}_2\text{(amine)} \rightarrow \text{Si–O–N}^+\text{N}_3\text{R}$$

$$\text{CO}_2 + 2\text{RNH}_2 \rightarrow =\text{RNHCOO}^- + \text{RNH}_3^+$$

### 4.8. Concept of $CO_2$-based fertilizer

Desert sand poses significant challenges for plant growth due to its lack of essential nutrients, poor water retention, and unfavorable soil structure. These factors, combined with the harsh environmental conditions of desert regions, make it extremely difficult for plants to establish and thrive. The approach of using small portions of the fertilizer is particularly noteworthy, as it allows for the improvement of growing conditions while minimally altering the overall desert ecosystem. This innovative fertilizer solution has the potential to transform arid regions, making them more suitable for agriculture or reforestation efforts. By addressing the fundamental limitations of desert sand, it opens up new possibilities for sustainable plant growth in challenging environments, potentially contributing to food security, land reclamation, and ecological restoration in arid and semi-arid regions around the world.

**4.8.1. Experimental setup for plant growth.** To prepare the experimental formulations for testing the effectiveness of various adsorbents in promoting plant growth, pure sand was combined with each type of absorbent in specific ratios (Table 2). The measured amounts of each sample were crushed and mixed with sand using a roller mixer |SRT9 D| mechanical mixer at 47 rpm to ensure uniform distribution of the adsorbent throughout the growing medium (Fig. 8(a)). This thorough mixing was essential to create a consistent substrate that would provide reliable results during the plant growth trials. The samples after mixing with sand were coded as S-PK, S-CKP-0, S-CKP-30, and S-CKP-50 (Fig. 8(b)).

Once the mixtures were prepared, they were transferred into cone-like containers made from plastic bottles. These containers served as planting vessels for the coriander seeds, which were selected for the seedling trials. The container seeds were then placed inside a hydroponic apparatus Z216 (17 pods) (Product Model: Z216) providing a controlled environment for the seedlings. The hydroponic system was designed to simulate desert conditions while providing precise control over environmental factors. The apparatus was closed to maintain a controlled environment (Fig. 8(c)), with temperature monitored using a calibrated thermometer (Fig. 8(d)). Light intensity within the system was measured accurately using a digital lux meter (Fig. 8(e)), ensuring optimal illumination for plant growth.

To create a more realistic desert-like substrate, a sand bed was incorporated into the hydroponic system. This sand layer served multiple purposes:

- It provided ample space for root penetration and growth.
- It simulated the natural environment of desert plants.
- It offered support and stability for the developing root systems.

Table 2 The code and compositions of all prepared samples

| S. No. | Samples | Code | Composition |
|---|---|---|---|
| 1 | Pure kaolinite + sand | S-PK | PK (1 g) + sand (9 g) |
| 2 | CTAB modified kaolinite + sand | S-CKP-0 | CKP-0 (1 g) + sand (9 g) |
| 3 | PEI (30) impregnated/CTAB modified kaolinite + sand | S-CKP-30 | CKP30 (1 g) + sand (9 g) |
| 4 | PEI (50) impregnated/CTAB modified kaolinite + sand | S-CKP-50 | CKP50 (1 g) + sand (9 g) |

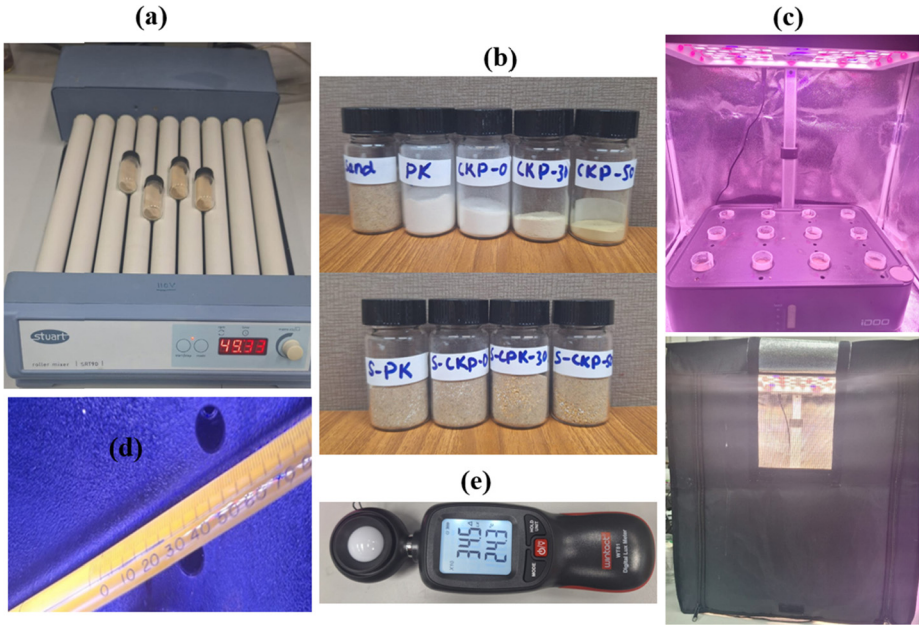


Fig. 8 (a) Digital photos of samples used in the current study: (a) sand, PK, CKP-0, CKP-30, and CKP-50, after mixing with sand coded as S-PK, S-CKP-0, S-30, and S-CKP-50, (b) roller mixer, (c) hydroponic apparatus use (open and closed), (d) thermometer for temperature measurement and (e) digital lux meter used to measure light intensity inside the hypophonic apparatus.

The seed containers were specially designed with open bottoms, allowing them to be partially submerged in the sand bed. This configuration enabled direct root contact with the substrate, mimicking natural growing conditions more closely. To maintain consistent moisture levels crucial for plant development, a precise irrigation schedule was implemented. Each container received 2 mL of water at regular intervals over the course of the 50-day experiment. This controlled watering regimen ensured that the plants received adequate hydration while still experiencing conditions like their native arid environments.

**4.8.2. Evaluation of plant growth.** Table 3 presents the growth data of coriander plants over a 55-day period using prepared $CO_2$ based fertilizers, including pure S-PK, S-CKP-0, S-CKP-30, and S-CKP-50. Throughout this period, the plants were monitored for growth and development, allowing for a detailed evaluation of how each adsorbent formulation influenced plant health and height. Several parameters including height were measured to evaluate the effectiveness of each adsorbent in promoting plant growth. These included plant height, and overall health of the plants. Fig. 9(a)–(f) presents the digital photos of stages of plant growth in a hydroponic apparatus, starting from the seed sowing day (Fig. 9(a)) over a period of 55 days. Germination started except with S-PK after 5 days (Fig. 9(b)) and stem development began after 10 days and marking the early growth phase. Significant growth was observed after 15 days (Fig. 9(d)), and noticeable development was observed. By day 20 (Fig. 9(e)), the plants reached good height, with further growth continuing by day 25 (Fig. 9(f)). The maximum height was achieved by day 30 (Fig. 9(g)), representing the full growth of the plants. After that the plants started to mature and their leaves become thinner (Fig. 9(h)), and after 45 days flowers also started to appear (Fig. 9(i)). After that the seed became developed as observed in 55 days of sowing (Fig. 9(j)).

Table 3 Coriander plant growth over a 30-day period with different adsorbents

| Time | Adsorbent for plant growth height (cm) | | | |
|---|---|---|---|---|
| Days | S-PK | S-CKP-0 | S-CKP-30 | S-CKP-50 |
| 0 | 0 | 0 | 0 | 0 |
| 5 | 1.1 | 1.3 | 2.1 | 3.1 |
| 10 | 3.2 | 4.3 | 6.3 | 7.24 |
| 15 | 6.1 | 8.5 | 10.3 | 12.2 |
| 20 | 7.2 | 9.3 | 14.2 | 16.2 |
| 25 | 8.3 | 11.2 | 20.1 | 22.1 |
| 30 | 9.1 | 13.1 | 25.1 | 27.1 |

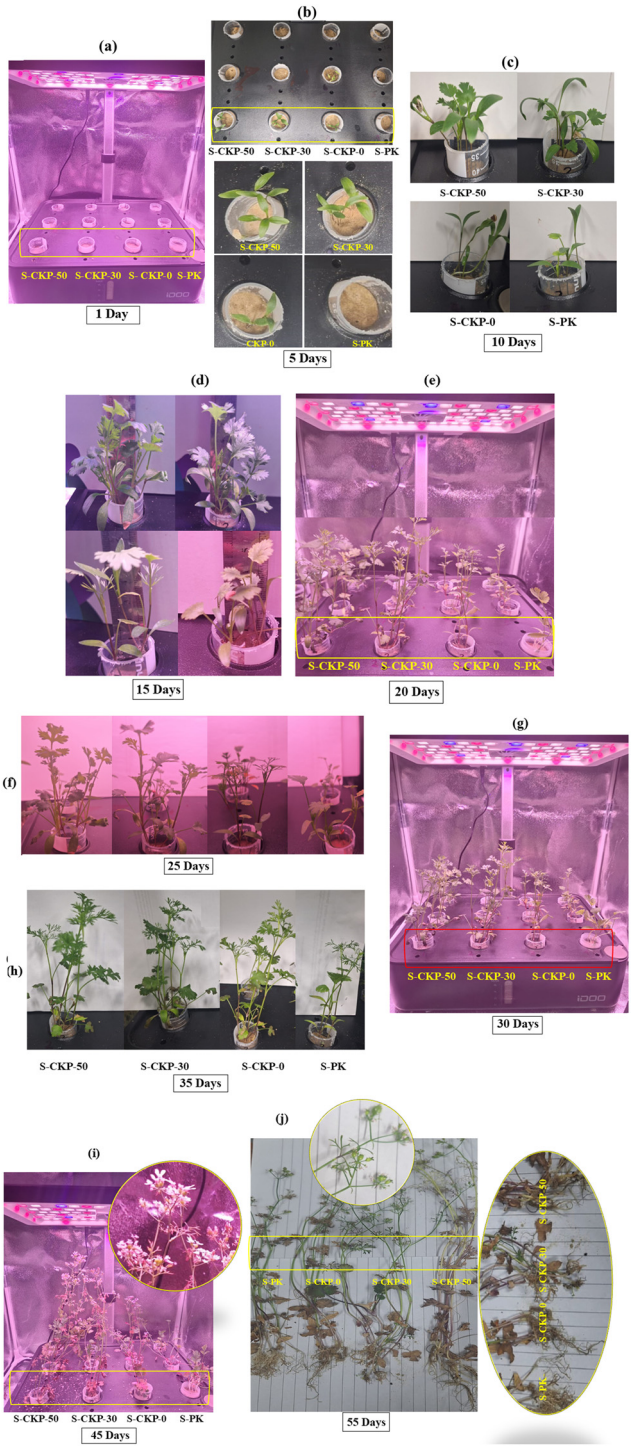


Fig. 9 (a–j) Plant growth experiment in hydroponic apparatus over a 55-day period, illustrating controlled growth stages from germination to maturity.

The height of plant growth for each adsorbent was noted for the period of 30 days as after that the height become constant. The height for each fertilizer was measured after each 5 days and the results are presented in Fig. 10 for (a) S-PK, (b) S-CKP-0, (c) S-CKP-30 and (d) S-CKP-50. While comparison of height for each sample is given in Fig. 10(e). The height for each adsorbent after 5 days was as follows: S-PK (1.1 cm), S-CKP-0 (1.3 cm), S-CKP-30 (2.1 cm), and S-CKP-50 (3.1 cm). Significant growth was observed after 10 days: S-PK (3.2 cm), S-CKP-0 (4.3 cm), S-CKP-30 (6.3 cm), and S-CKP-50 (7.24 cm). By day 20 the plants reached: S-PK (7.2 cm), S-CKP-0 (9.3 cm), S-CKP-30 (14.2 cm), and S-CKP-50 (16.2 cm). The growth continued, with the following heights by day 25: S-PK (8.3 cm), S-CKP-0 (11.2 cm), S-CKP-30 (20.1 cm), and S-CKP-50 (22.1 cm). The maximum height was achieved by day 30 with the final heights recorded as: S-PK (9.1 cm), S-CKP-0 (13.1 cm), S-CKP-30 (25.1 cm), and S-CKP-50 (27.1 cm). The maximum height for each adsorbent is given in Fig. 10(f). These results showed that the maximum height was achieved by day 30 by S-CKP-50 representing the full growth of the plant.

**4.8.3. Explanation.** Pure kaolinite (PK) clay with sand may not support plant growth effectively due to several key factors. PK has a relatively low cation exchange capacity (CEC), which limits its ability to retain water, leading to dry conditions that are unfavorable for plant growth. Plants need adequate moisture to thrive, and PK's low moisture retention is a significant disadvantage. The soil structure of unmodified kaolinite can also be problematic. Its fine particle size may lead to compaction, reducing aeration and impeding root development. The pH levels of unmodified kaolinite can further complicate its suitability for plant growth. Depending on its composition, kaolinite can be too acidic or too alkaline for many plant species, affecting nutrient availability and overall plant health. This indicates that while kaolinite provides some basic support, its ability to promote significant growth in coriander plants is limited due to the lack of chemical modifications that enhance nutrient or moisture retention. Additionally, the $CO_2$ adsorption capacity of PK is low, which means that it cannot significantly increase soil fertility for plant growth.

CTAB-modified kaolinite (CK) with sand offers several advantages that enhance plant growth compared to unmodified kaolinite. The modification with cetyltrimethylammonium bromide (CTAB) improves the clay's properties, making it more suitable for agricultural applications. CK modification increases the CEC of kaolinite, alters its surface characteristics, and promotes better water retention and moisture availability. The enhanced pore structure improves aeration and drainage, both beneficial for healthy root development.

The structural integrity of CK also helps prevent soil compaction, allowing better root penetration and overall plant stability. Furthermore, the $CO_2$ adsorption capacity of CK is higher than that of PK, increasing soil fertility to some extent and supporting plant growth. The introduction of PEI at a 30% loading level into kaolinite (CKP30) and use with sand brought some benefits, improving plant growth compared to S-PK and S-CKP-0. The 30% PEI loading enhanced the surface characteristics and water retention properties of kaolinite, improving moisture availability for the plants. The $CO_2$ adsorption capacity of CKP30 is higher than that of PK and CK, leading to better plant growth as the increased $CO_2$ boosts fertility and provides essential nutrients. The addition of 30 wt% PEI enhances the adsorption capacity of kaolinite, potentially improving nutrient

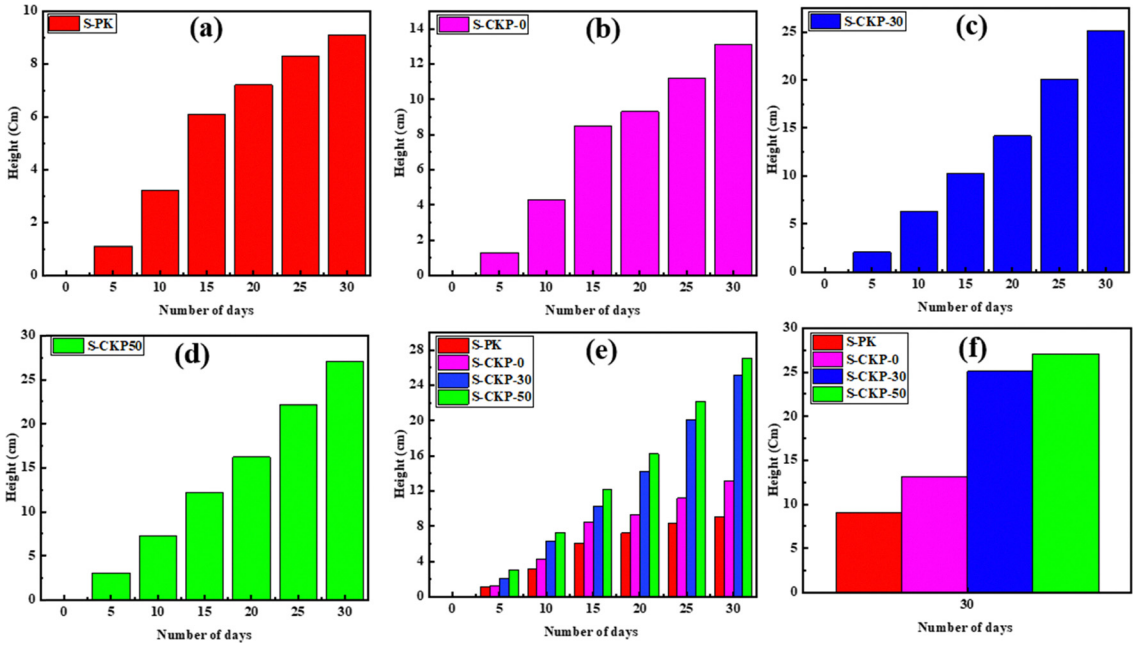


Fig. 10 Height profile of (a) S-PK, (b) S-CKP-0, (c) S-CKP-30 and (d) S-CKP-50 over a period of 30 days, (e) comparison of height for each sample, (f) maximum height of all prepared adsorbents over 30 days.

and water retention in the soil, which directly benefits the growth of coriander plants. The higher concentration of PEI further enhances the interaction between the adsorbent and the plant roots, improving the soil's moisture retention, nutrient availability, and overall growth environment. The 50% PEI loading in CKP50 and use with sand resulted in the most significant improvements in plant growth among all the tested materials. With this higher PEI concentration, kaolinite exhibited optimal water retention, nutrient retention, and aeration properties. The enhanced moisture retention and improved soil structure provided ideal conditions for root development and overall plant growth. S-CKP50 also displayed superior ability to prevent soil compaction, allowing better root penetration and stability. Most notably, CKP50's higher $CO_2$ adsorption capacity further increased soil fertility, providing additional nutrients to support healthy plant growth, making it the most effective material for promoting plant growth. This indicates that 50 wt% PEI provides the most effective modification for optimal coriander plant growth.

In conclusion, the results show that PEI-modified kaolinites (S-CKP-30 and S-CKP-50) significantly improve coriander plant growth compared to pure kaolinite and CTAB-modified kaolinite. The higher the PEI content, the greater the enhancement in plant height, with S-CKP-50 yielding the best results at 27.1 cm. These findings suggest that PEI-modified clay adsorbents are highly effective in improving plant growth, particularly by enhancing the soil's ability to retain moisture and nutrients, thus providing a promising solution for agricultural applications.

## 5. Conclusion

The transformation of desert sands into fertile land using $CO_2$ adsorbed on clays offers a promising and innovative solution to combat desertification and mitigate climate change. In this study, we prepared a $CO_2$-enriched fertilizer with the potential to combat desertification and $CO_2$ adsorption. Initially, kaolinite was modified using cetyltrimethylammonium bromide (CTAB) and then impregnated with varying concentrations of polyethyleneimine (PEI). The prepared adsorbents were thoroughly analysed using various characterization techniques, including Fourier transform infrared spectroscopy (FTIR), X-ray diffraction (XRD), scanning electron microscopy (SEM), and transmission electron microscopy (TEM). These methods helped in assessing the structural properties and morphology of the modified kaolinite. The adsorbents were tested for $CO_2$ uptake capacity as well as their potential to support plant growth. The results demonstrated that $CO_2$-enriched clays offer a cost-effective and environmentally sustainable solution for $CO_2$ adsorption while significantly enhancing plant growth compared to pure kaolinite clay. Among all the adsorbents, those with amine loadings, particularly S-CKP30 (30% PEI) and S-CKP50 (50% PEI), showed substantial improvements in plant growth relative to both pure kaolinite and CTAB-modified kaolinite. Notably, S-CKP50, produced the most favorable results. These results showed that $CO_2$-enriched clays, especially those modified with PEI, represent an effective and sustainable approach to both $CO_2$ capture and desert reclamation. CKP50, in particular, stands out as an ideal candidate for improving soil conditions, supporting plant growth, and offering long-term environmental benefits, making it a promising solution for combating desertification and addressing the global challenges of climate change.

## Data availability

The datasets generated and analysed during this study are available from the corresponding author upon reasonable request.

Additional information and materials related to the research are provided in the ESI,† where applicable.

## Conflicts of interest

There are no conflicts to declare.

## References

1 H. W. Ku, *et al.*, ''Active'' hydroponic greenhouse system to kick-start and augment reforestation program through carbon sequestration–an experimental and theoretical feasibility study, *J. Cleaner Prod.*, 2016, **129**, 637–646.
2 E. Kawai, A. Ozawa and B. D. Leibowicz, Role of carbon capture and utilization (CCU) for decarbonization of industrial sector: A case study of Japan, *Appl. Energy*, 2022, **328**, 120183.
3 M. Yusuf and H. Ibrahim, A comprehensive review on recent trends in carbon capture, utilization, and storage techniques, *J. Environ. Chem. Eng.*, 2023, 111393.
4 J. Podder, *et al.*, A review of carbon capture and valorization technologies, *Energies*, 2023, **16**(6), 2589.
5 K. Zhao, *et al.*, Recent advances and future perspectives in carbon capture, transportation, utilization, and storage (CCTUS) technologies: A comprehensive review, *Fuel*, 2023, **351**, 128913.
6 U. S. D'Ettorre, I. S. Liso and M. Parise, Desertification in karst areas: A review, *Earth-Sci. Rev.*, 2024, 104786.
7 S. Zhang, *et al.*, Research Progress on Ecological carrying Capacity and Ecological Security, and its inspiration on the forest ecosystem in the Karst Desertification Control, *Forests*, 2024, **15**(9), 1632.
8 M. A. AbdelRahman, An overview of land degradation, desertification and sustainable land management using GIS and remote sensing applications, *Rend. Lincei, Sci. Fis. Nat.*, 2023, **34**(3), 767–808.
9 D. Shanmugavel, *et al.*, Sustainable SMART fertilizers in agriculture systems: A review on fundamentals to in-field applications, *Sci. Total Environ.*, 2023, **904**, 166729.
10 S. Liu, *et al.*, Simultaneously tackling ecological degradation and poverty challenges: Evidence from desertified areas in northern China, *Sci. Total Environ.*, 2022, **815**, 152927.
11 A. Yussupov and R. Z. Suleimenova, Use of remote sensing data for environmental monitoring of desertification, *Evergreen: Jt. J. Novel Carbon Resour. Sci. Green Asia Strategy*, 2023, 300–307.
12 M. Pizzol, J. C. Smart and M. Thomsen, External costs of cadmium emissions to soil: a drawback of phosphorus fertilizers, *J. Cleaner Prod.*, 2014, **84**, 475–483.
13 T. Gomiero, D. Pimentel and M. G. Paoletti, Environmental impact of different agricultural management practices: conventional *vs.* organic agriculture, *Crit. Rev. Plant Sci.*, 2011, **30**(1–2), 95–124.
14 N. Mushtaq, *et al.*, Freshwater contamination: sources and hazards to aquatic biota, *Fresh water pollution dynamics and remediation*, 2020, pp. 27–50.
15 M. A. Dervash, *et al.*, Biotechnological intervention as an aquatic clean up tool, *Fresh water pollution dynamics and remediation*, 2020, pp. 183–196.
16 G. H. Dar, *et al.*, *Microbiota and biofertilizers*, Springer, 2021, vol. 2.
17 R. Dinesh, *et al.*, Short-term incorporation of organic manures and biofertilizers influences biochemical and microbial characteristics of soils under an annual crop [Turmeric (*Curcuma longa* L.)], *Bioresour. Technol.*, 2010, **101**(12), 4697–4702.
18 G. Dar, *et al.*, Characterization of Aeromonas sobria isolated from fish Rohu (Labeo rohita) collected from polluted pond, *J. Bacteriol. Parasitol.*, 2016, **7**(3), 1–5.
19 G. M. Shah, *et al.*, Toxicity of ZnO and $Fe_2O_3$ nano-agro-chemicals to soil microbial activities, nitrogen utilization, and associated human health risks, *Environ. Sci. Eur.*, 2022, **34**(1), 106.
20 T. G. Abebe, *et al.*, Growing use and impacts of chemical fertilizers and assessing alternative organic fertilizer sources in Ethiopia, *Appl. Environ. Soil Sci.*, 2022, **2022**(1), 4738416.
21 A. K. Shukla, *et al.*, Fertilizer use in Indian agriculture and its impact on human health and environment, *Indian J. Fert.*, 2022, **18**(3), 218–237.
22 Y. Guo and J. Wang, Spatiotemporal changes of chemical fertilizer application and its environmental risks in China from 2000 to 2019, *Int. J. Environ. Res. Public Health*, 2021, **18**(22), 11911.
23 W. Ouyang, *et al.*, Increased ammonia emissions from synthetic fertilizers and land degradation associated with reduction in arable land area in China, *Land Degrad. Dev.*, 2018, **29**(11), 3928–3939.
24 A. M. Ghanem, *et al.*, Measuring impact of air and agricultural soil pollution on social development in Saudi Arabia, *J. Exp. Biol. Agric. Sci.*, 2022, 575–583.
25 W. Al-Busaidi, *et al.*, Impact of long-term agricultural farming on soil and water chemical properties: A case study from Al-Batinah regions (Oman), *J. Saudi Soc. Agric. Sci.*, 2022, **21**(6), 397–403.
26 M. Sulaiman, *et al.*, Accumulation of toxic elements in soil and date palm (*Phoenix dactylifera* L.) through fertilizer application, *J. Plant Nutr.*, 2021, **44**(7), 958–969.
27 A. A. Al-Taani, *et al.*, Contamination assessment of heavy metals in agricultural soil, in the Liwa area (UAE), *Toxics*, 2021, **9**(3), 53.
28 S. Jain, *et al.*, Global-scale water security and desertification management amidst climate change, *Environ. Sci. Pollut. Res.*, 2024, 1–25.
29 S. Velioglu and S. Keskin, Revealing the effect of structure curations on the simulated $CO_2$ separation performances of MOFs, *Mater. Adv.*, 2020, **1**(3), 341–353.
30 S. Samanta and R. Srivastava, Catalytic conversion of $CO_2$ to chemicals and fuels: the collective thermocatalytic/photocatalytic/electrocatalytic approach with graphitic carbon nitride, *Mater. Adv.*, 2020, **1**(6), 1506–1545.
31 M. J. Nazir, *et al.*, Harnessing soil carbon sequestration to address climate change challenges in agriculture, *Soil Tillage Res.*, 2024, **237**, 105959.

32 M. Vinoba, *et al.*, Exploring Enthalpies of $CO_2$ and $N_2$ Adsorption on Zn-and Co-Based Zeolitic Frameworks at Varying Temperatures and Pressures, *Results Eng.*, 2024, 103582.
33 J. D. Souza-Filho, *et al.*, Zeolite A grown on fiberglass: A prominent $CO_2$ adsorbent for $CO_2/CH_4$ separation, *Colloids Surf., A*, 2024, **683**, 132952.
34 B. Mohan, *et al.*, Carbon dioxide capturing activities of porous metal-organic frameworks (MOFs), *Microporous Mesoporous Mater.*, 2024, **366**, 112932.
35 P. Anantharamu, *et al.*, Improved metal-organic frameworks (MOFs) and their application in catalytic $CO_2$ reduction: A review, *Mater. Today Sustainability*, 2024, 100745.
36 N. H. Khdary, *et al.*, Metal oxides as catalyst/supporter for $CO_2$ capture and conversion, review, *Catalysts*, 2022, **12**(3), 300.
37 F. Fathalian, *et al.*, Efficient $CO_2$ adsorption using chitosan, graphene oxide, and zinc oxide composite, *Sci. Rep.*, 2024, **14**(1), 3186.
38 S. Wang, *et al.*, Recent advances in capture of carbon dioxide using alkali-metal-based oxides, *Energy Environ. Sci.*, 2011, **4**(10), 3805–3819.
39 H. Zeng, *et al.*, Porous adsorption materials for carbon dioxide capture in industrial flue gas, *Front. Chem.*, 2022, **10**, 939701.
40 B. Dziejarski, J. Serafin and K. Andersson, $CO_2$ capture materials: a review of current trends and future challenges, *Mater. Today Sustainability*, 2023, 100483.
41 B. Dziejarski, *et al.*, Activated carbons—Preparation, characterization and their application in $CO_2$ capture: A review, *Environ. Sci. Pollut. Res.*, 2023, **31**(28), 40008–40062.
42 N. A. Rashidi and S. Yusup, Potential of palm kernel shell as activated carbon precursors through single stage activation technique for carbon dioxide adsorption, *J. Cleaner Prod.*, 2017, **168**, 474–486.
43 M. Danish, V. Parthasarthy and M. K. Al Mesfer, $CO_2$ capture by low-cost date pits-based activated carbon and silica gel, *Materials*, 2021, **14**(14), 3885.
44 A. E. Ogungbenro, *et al.*, Physical synthesis and characterization of activated carbon from date seeds for $CO_2$ capture, *J. Environ. Chem. Eng.*, 2018, **6**(4), 4245–4252.
45 A. S. Ello, *et al.*, Coconut shell-based microporous carbons for $CO_2$ capture, *Microporous Mesoporous Mater.*, 2013, **180**, 280–283.
46 R. Sanz, *et al.*, $CO_2$ adsorption on branched polyethyleneimine-impregnated mesoporous silica SBA-15, *Appl. Surf. Sci.*, 2010, **256**(17), 5323–5328.
47 H. Zhu, *et al.*, A highly effective and low-cost sepiolite-based solid amine adsorbent for $CO_2$ capture in post-combustion, *Sep. Purif. Technol.*, 2023, **306**, 122627.
48 Y.-H. Chen and D.-L. Lu, $CO_2$ capture by kaolinite and its adsorption mechanism, *Appl. Clay Sci.*, 2015, **104**, 221–228.
49 L. Wang, *et al.*, Amine-modified ordered mesoporous silica: The effect of pore size on $CO_2$ capture performance, *Appl. Surf. Sci.*, 2015, **324**, 286–292.
50 A. E. Elkhalifah, *et al.*, Carbon dioxide retention on bentonite clay adsorbents modified by mono-, di-and triethanolamine compounds, *Adv. Mater. Res.*, 2014, **917**, 115–122.
51 J. Hou, *et al.*, Regulating the effect of element doping on the $CO_2$ capture performance of kaolinite: A density functional theory study, *Appl. Surf. Sci.*, 2020, **512**, 145642.
52 Q. Liu, *et al.*, Preparation of ZSM-5 molecular sieve modified by kaolin and its $CO_2$ adsorption performance investigation, *Microporous Mesoporous Mater.*, 2023, **360**, 112678.
53 F. Bahmanzadegan, M. A. Pordsari and A. Ghaemi, Improving the efficiency of 4A-zeolite synthesized from kaolin by amine functionalization for $CO_2$ capture, *Sci. Rep.*, 2023, **13**(1), 12533.
54 S. O. Akpasi and Y. M. Isa, Effect of operating variables on $CO_2$ adsorption capacity of activated carbon, kaolinite, and activated carbon–Kaolinite composite adsorbent, *Water-Energy Nexus*, 2022, **5**, 21–28.
55 L. Stevens, *et al.*, Preparation and $CO_2$ adsorption of diamine modified montmorillonite via exfoliation grafting route, *Chem. Eng. J.*, 2013, **215**, 699–708.
56 Y.-H. Chen and D.-L. Lu, Amine modification on kaolinites to enhance $CO_2$ adsorption, *J. Colloid Interface Sci.*, 2014, **436**, 47–51.
57 J. Liu, *et al.*, Polyethyleneimine functionalized protonated titanate nanotubes as superior carbon dioxide adsorbents, *J. Colloid Interface Sci.*, 2012, **386**(1), 392–397.
58 W. Pi, *et al.*, Carbon dioxide adsorption capacity of porous carbon after polyamine impregnation under different pore structures and temperatures, *Chem. Eng. J.*, 2024, **485**, 150025.
59 M. S. Salman, *et al.*, Improving copper(II) ion detection and adsorption from wastewater by the ligand-functionalized composite adsorbent, *J. Mol. Struct.*, 2023, **1282**, 135259.
60 A. S. Chong, M. A. Manan and A. K. Idris, Sodium lignosulfonate as sacrificial agent and effectiveness in reducing CTAB cationic adsorption onto kaolinite, *J. King Saud Univ., Eng. Sci.*, 2021, **33**(8), 539–546.
61 R. Duarte-Silva, *et al.*, Structural, textural and protein adsorption properties of kaolinite and surface modified kaolinite adsorbents, *Appl. Clay Sci.*, 2014, **90**, 73–80.
62 V. C. Khang, M. V. Korovkin and L. G. Ananyeva, Identification of clay minerals in reservoir rocks by FTIR spectroscopy, *IOP Conference Series: Earth and Environmental Science*, IOP Publishing, 2016.
63 Y. Li, *et al.*, Effective removal of emulsified oil from oily wastewater using surfactant-modified sepiolite, *Appl. Clay Sci.*, 2018, **157**, 227–236.
64 N. Belachew and H. Hinsene, Preparation of cationic surfactant-modified kaolin for enhanced adsorption of hexavalent chromium from aqueous solution, *Appl. Water Sci.*, 2020, **10**(1), 1–8.
65 Z. Li, Z. Pan and Y. Wang, Mechanochemical preparation of ternary polyethyleneimine modified magnetic illite/smectite nanocomposite for removal of Cr(VI) in aqueous solution, *Appl. Clay Sci.*, 2020, **198**, 105832.
66 M. S. Żbik, *et al.*, Kaolinite platelet orientation for XRD and AFM applications, *Appl. Clay Sci.*, 2010, **50**(3), 299–304.
67 A. Kumar and P. Lingfa, Sodium bentonite and kaolin clays: Comparative study on their FT-IR, XRF, and XRD, *Mater. Today: Proc.*, 2020, **22**, 737–742.

68 M. Shaban, *et al.*, Adsorption behavior of inorganic-and organic-modified kaolinite for Congo red dye from water, kinetic modeling, and equilibrium studies, *J. Sol-Gel Sci. Technol.*, 2018, **87**, 427–441.
69 H. Ahmadizadegan and S. Esmaielzadeh, Organically modified clay as an enhancement filler in novel polyimide mixed matrix membranes for gas separation, *Polym. Bull.*, 2024, **81**(4), 3273–3296.
70 L. Zhu and R. Zhu, Simultaneous sorption of organic compounds and phosphate to inorganic–organic bentonites from water, *Sep. Purif. Technol.*, 2007, **54**(1), 71–76.
71 S. M. Lee and D. Tiwari, Porous hybrid materials in the remediation of water contaminated with As(III) and As(V), *Chem. Eng. J.*, 2015, **270**, 496–507.
72 J. Ouyang, *et al.*, Polyethyleneimine (PEI) loaded MgO-SiO2 nanofibers from sepiolite minerals for reusable $CO_2$ capture/release applications, *Appl. Clay Sci.*, 2018, **152**, 267–275.
73 J. Cheng, *et al.*, Polyethyleneimine entwine thermally-treated Zn/Co zeolitic imidazolate frameworks to enhance $CO_2$ adsorption, *Chem. Eng. J.*, 2019, **364**, 530–540.